# Fusion hindrance at deep sub-barrier energies

Ajit Kumar Mohanty*
*Nuclear Physics Division, Bhabha Atomic Research Centre, Mumbai 400 085, India*
(Dated: February 1, 2008)

Fusion of two heavy nuclei may be initiated at larger distances (before contact point is reached) due to neck formation or due to strong neutron flow between the two colliding nuclei leading to an elongated di-nuclear configuration. When injected into the adiabatic fusion trajectory, these configurations undergo further up hill diffusion to achieve fusion, thus causing fusion hindrance at deep sub-barrier energies. Coupled channel calculations based on this new concept is able to explain the measured steep falloff in fusion cross sections and associated anomalies at deep sub-barrier energies. Further, it is also shown that fusion initiated by neutron flow followed by diffusion can provide a natural explanation to fusion of radioactive ions charcterirzed by extended neutron halos, a topic which is highly controversial.

PACS numbers: PACS numbers:25.70.Jj24.10.Eq,25.60.-t,25.70.Gh



## I. INTRODUCTION

The study of near and sub-barrier fusion of heavy and exotic ions have generated a considerable amount of interest and anomalies over the last several years. In the simplest picture, fusion reaction between two ions at sub-barrier energies is governed by the penetration through the Columb barrier followed by an absorption inside the barrier. Early anomalies refer to the failure of this simple barrier penetration model (BPM) which could not explain the large enhancement found in the measurement of fusion cross sections for all heavy ion systems particularly at sub-barrier energies [1, 2]. Since then, several theoretical models have been proposed to account for this large sub-barrier enhancement. The most successful model that has emerged out of these studies over the past several years is the description of fusion within a coupled channel framework where the presence of couplings to various low lying inelastic and transfer channels are treated explicitly. Under certain approximation, the channel couplings can be interpreted as a phenomena by which the colliding nuclei encounter a distribution of barriers, one or more of which having height less than the original Coulomb barrier, thus giving large fusion enhancement. Therefore, a better understanding of the fusion process followed through the distribution of barriers which can be derived experimentally from the second derivative of the product of the fusion cross section with energy [3]. In most experiments, fusion cross sections have been measured down to the $1-0.1mb$ level and the coupled channel calculations have been quite successful in reproducing the general trends of the measured yields. While efforts are still being put to improve upon the techniques of these calculations to understand the nature of fusion enhancement and the associated barrier distribution, some of the recent measurements at extreme sub-barrier energies [4, 5] (cross section below the $\mu b$ level for systems like $^{64}Ni+^{64}Ni$, $^{58}Ni+^{58}Ni$, $^{60}Ni+^{89}Y$) have brought out new surprises which show supression in fusion cross section with respect to the same coupled channel calculations that explains the enhancement at sub-barrier energies. The most striking feature of these measurements are the logarithimic derivative $L(E) = d(ln\sigma E)/dE$ which continues to increase steeply with decreasing energies where as all the realistic model calculations including that of coupled channel results predict a slow rise in $L(E)$ or eventually tends to saturate to a constant value [6, 7, 8]. All these models also fail to explain the behavior of $S$-factor which shows the presence of a maximum indicating a strong hindrance to fusion at deep sub-barrier energies [5, 7].

Recently, these anomalies have been explained successfully by using a drastically modified nuclear potential in the barrier region that results in a shawlloer potential pocket as wll as a thicker potential barrier [9, 10]. While the thicker barrier is responsible for the steep falloff of the fusion cross secion at deep sub-barrier energies, the shallower potential pocket prevents higher partial waves to fuse. Although the proposed concept is highly illuminating and has several new features [10] that requires further experimental investigations, the model suffers from one technical draw back due to the existence of a higher cut-off energy below which the system will not be able to fuse. For example, in case of $^{64}Ni+^{64}Ni$ system, the minimum value of the potenial pocket $V_{min} \approx 85$ MeV which is about 9 MeV below the Coulomb barrier. This would imply that fusion cross section $\sigma_f$ will vanish for $E_{cm} \leq V_{min}$ although compound nucleus formation is still possible as long as $(E_{cm}+Q)$ is positive i.e. compound nucleus can in principle be formed down to a threshold energy of $E_{cm} \approx 49$ MeV. The experimental measurements also do not suggest a sharp cut-off in $\sigma_f$ for $E_{cm} \leq V_{min}$. Therefore, without putting any stringent requirement to modify the nuclear potential at the interior of the Coulomb barrier, we propose an alternate model, yet very sinple to implement within a coupled channel frame work, by allowing fusion to initiate through neutron flow or through neck formation at a dis-

*Electronic address: ajitkm@barc.gov.in

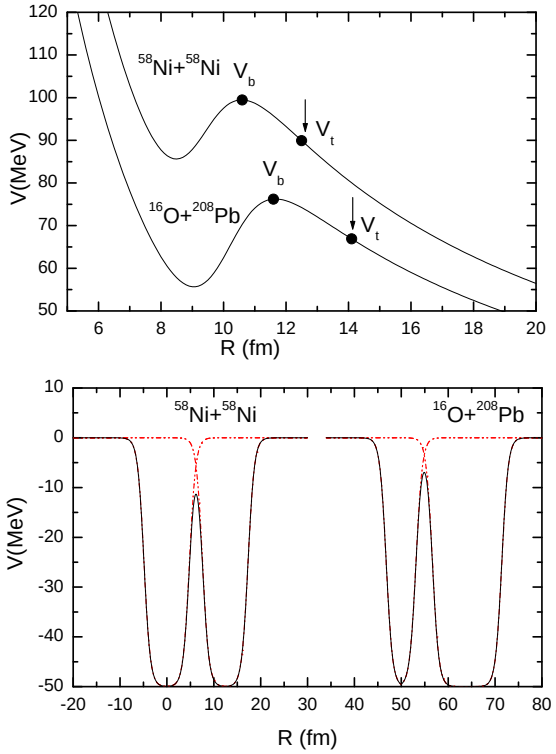


FIG. 1: (Upper panel) The potential $V(R)$ versus inter-nuclar distance $R$ for $^{58}Ni+^{58}Ni$ and $^{16}O+^{208}Pb$ systems. Lower panel shows the two centre shell model potentials for individual nuclei (dashed-dot curves in red) and merged neutron potentials (solid curves) for $^{58}Ni+^{58}Ni$ and $^{16}O+^{208}Pb$ systems at distances of 12.5 fm and 14.1 fm respectively. In the lower panel, x-axis has been shifted by 50 fm for clarity for $^{16}O+^{208}Pb$ system.

tance much before the Coulomb barier is reached. Since these di-nuclear complexes (two nuclei connected by a thin neck) are formed at large distances, further up hill diffusion over an adiabatic fusion trajectory is required in order to achieve fusion. This new concept not only able to explain recent experimental anomalies at deep sub-barrier energies, but also it accounts for the general trends of fusion process for several heavy ion systems over a wide range of energies starting from above to deep sub-barrier energeis. Contrary to the general expectation that the two nuclei will fuse by tunneling through the Coulomb barrier, the fusion in the present model is proposed to be initiated by neutron flow at large distances followed by disffusion over the Coulomb barrier. Interestingly, apart from heavy ion systems, this model also explains fusion phenomena of radio active nuclei (having extended neutron halos) in a natural way, a topic which is highly controversial [11, 12, 13, 14, 15, 16].

It is the normal practice to assume that the colliding nuclei will fuse tunneling through the barrier when $E < V_b$ where $V_b$ is the height of the Coulomb barrier. Fig. 1 (upper panel) shows the plots of total potential as a function of inter nuclear distance $R$ for two typical ($^{58}Ni+^{58}Ni$ and $^{16}O+^{208}Pb$) systems. It may be mentioned here that when the colliding nuclei approach each other, this Coulomb barrier provides a respulsive force to the proton clouds only and does not prevent neutrons to flow from one nuclei to other. In fact, it was argued by Stelson [17] earlier that fusion may be initiated at large distances when it is possible for neutrons to flow between the colliding nuclei. This we investigate for a few systems by using the neutron shell model potentials as was used in [17]. We assume a Woods-Saxon shape with $V = V_0/\{1 + exp[(R - R_0)/a]\}$, where $V_0 = -50$ MeV, $R_0 = 1.24A^{1/3}$ fm, and $a = 0.68$ fm. Fig. 1 (lower panel) shows the example of the neutron potentials for $^{64}Ni+^{64}Ni$ and $^{16}O+^{208}Pb$ systems centered on each nuclei (dashed-dot curves in red) as well as the merged neutron potentials (solid curves) at a distances of 12.5 fm and 14.1 fm respectively. We take one half of the two neutron separation energy $S(2n)/2$ as an approximate measure of the binding energy of the valence neutrons. We estimate $S(2n)/2 \approx 11.2$ MeV and $S(2n)/2 \approx 7.0$ MeV for above two systems. In the figure, the inter nuclear separation has been adjusted to 12.5 fm and 14.1 fm respectively so that the barrier of the merged potential is deeper by the corersponding $S(2n/2)$ values. This is the situation when there is no barrier and the neutrons can flow freely. This distance $R_t$ is the thrshold distance (marked by the arrow in the upper figure) below which there is no barrier for neutrons to flow. In terms of energy, there is a threshold energy $E = V_t$ (the total potential at $R = R_t$) above which neutron flows freely and for $E < V_t$, neutrons need to tunnel through. In [4], from the experimental measureemnts, the authors have derived a thershold energy $E_t$ for a number of systems. The $E_t$ is the threshold enegy below which the fusion cross sections falls off steeply ($S$ factor shows a maxima). Fig. 2 shows the plot of $E_t$ (which are derived from the experimenal data [4] and listed in second column of table I) and $V_t$ for the same system estimated as described above. Interestingly, a strong correlation is found between the two threshold energies $E_t$ $V_t$ ($V_t \approx 0.95E_t$), which is an indication that neutrons flow may be acting as a door-way state for fusion [17, 18]. Macroscopically, it is equivalent to say that neutron flow provides a force strong enough to overcome the Coulomb replusion thus promoting neck formation and forming a di-nuclear complex at a distance away from the barrier position $R_b$. This neutron flow is rather sequencial and distinctly different from one or two neutron transfer which is generally treated as simultaneous coupling in the conventional coupled channel calculation [19]. These di-nuclear complexes can be best described as a swarm of Brownian particles suspended in a fluid at temperature $\Gamma$ instead of considering them as two separate entities approaching towords each other at a relative centre of mass energy $E_{cm}$. Although, some of the swarm will be sliding down due to replusive Coulomb force, because the swarm's width increases with time, the particles will diffuse up-hill and a

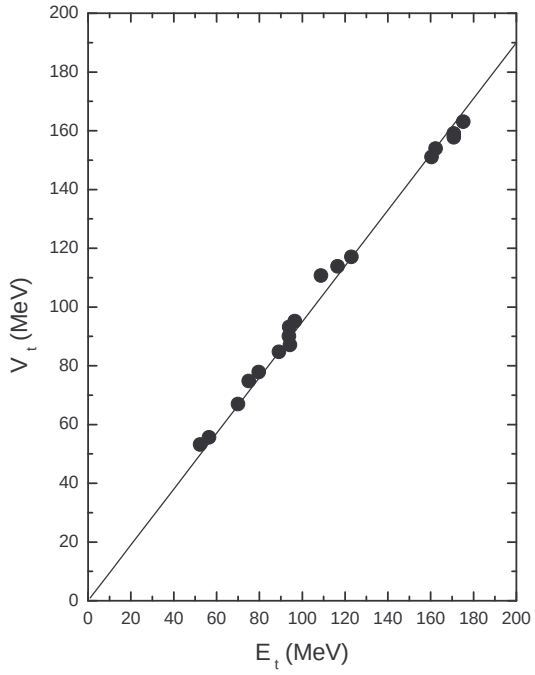


FIG. 2: Threshold potential $V_t$ (sixth column of thable I) versus threshold energy $E_t$ (fifth column of table I). The solid line is a linear fit to the data points ($V_t \approx 0.95E_t$).

TABLE I: The threshold energy and other relevant parameters for various systems. The strength of the nuclear potential has been adjusted to reproduced the same Columb barrier as used in Ref.[4] and are listed in the second column. The corresponding $R_b$ values are listed in the fourth column. The fifth column lists the threshold energy $E_t$ at which the $\sigma_f$ falls off steeply. The last two columns show the $V_t$ and $R_t$ values derived using the method as described in the text. Note that for all the systems, $R_t > R_b$ as expected.

| System | $V_b$ | $R_b$ | $S_{2n}/2$ | $E_t$ | $V_t$ | $R_t$ |
|---|---|---|---|---|---|---|
| $^{58}Ni + ^{58}Ni$ | 101.2 | 10.3 | 11.2 | 93.9 | 90.0 | 11.3 |
| $^{60}Ni + ^{89}Y$ | 132.5 | 11.1 | 10.2, 10.4 | 123.o | 117.1 | 13.4 |
| $^{90}Zr + ^{89}Y$ | 187.7 | 11.2 | 10.6, 10.4 | 170.8 | 159.0 | 14.1 |
| $^{90}Zr + ^{92}Zr$ | 189.6 | 11.3 | 10.6, 7.9 | 170.8 | 157.7 | 14.6 |
| $^{90}Zr + ^{90}Zr$ | 192.5 | 11.2 | 10.6 | 175.2 | 163.1 | 14.1 |
| $^{50}Ti + ^{208}Pb$ | 203.6 | 12.1 | 9.5, 7.1 | 181.6 | 167.5 | 15.5 |
| $^{64}Ni + ^{64}Ni$ | 98.0 | 10.7 | 8.2 | 89.2 | 84.7 | 13.3 |
| $^{16}O + ^{208}Pb$ | 76.3 | 11.7 | 14.4, 7.1 | 70.1 | 66.9 | 14.1 |
| $^{40}Ca + ^{90}Zr$ | 94.3 | 10.4 | 14.5, 7.9 | 94.3 | 87.1 | 13.2 |
| $^{16}O + ^{144}Sm$ | 56.6 | 10.9 | 14.4, 9.6 | 56.6 | 55.6 | 12.8 |
| $^{19}F + ^{208}Pb$ | 86.0 | 11.6 | 9.8, 7.1 | 75.1 | 74.7 | 14.2 |
| $^{16}O + ^{154}Sm$ | 60.6 | 11.0 | 14.4, 6.9 | 52.4 | 53.2 | 13.4 |
| $^{19}F + ^{208}Pb$ | 86.0 | 11.6 | 9.8, 7.1 | 75.1 | 74.7 | 14.2 |
| $^{40}Ar + ^{144}Sm$ | 133.5 | 11.1 | 8.2, 9.6 | 116.6 | 113.8 | 14.1 |
| $^{40}Ar + ^{154}Sm$ | 131.4 | 11.3 | 8.2, 6.9 | 108.8 | 110.7 | 14.5 |
| $^{40}Ar + ^{112}Sn$ | 110.6 | 10.9 | 8.2, 8.5 | 96.6 | 95.2 | 13.6 |
| $^{86}Kr + ^{92}Mo$ | 179.9 | 11.1 | 8.5, 11.4 | 160.4 | 151.0 | 14.4 |
| $^{86}Kr + ^{104}Ru$ | 185.9 | 11.5 | 8.5, 7.6 | 162.4 | 153.9 | 13.4 |
| $^{36}S + ^{110}Pd$ | 90.3 | 11.0 | 8.4, 7.5 | 79.7 | 77.8 | 13.5 |

fraction will be able to overcome the barrier and achieve fusion. As will shown later, fusion achieved through this diffusion process shows many interesting features that have been observed at deep sub-barrier energies.

The paper is organized as follows. After this brief introduction, in section II, we derive an expression for the one diemsnional diffusion model of fusion and compare the results with the predictions of the standard barrier penetration model. In section III, we propose a coupled channel formalism where fusion is estimated as a weighted sum over the distribution of barriers, but with a transmission factor estimated using the diffusion process. The results of the coupled channel calculations are compared with the experimental measurements. In section IV, we extend this formalism to explain experimental fusion cross sections of radio-active halo nuclei. Finally, the conclusions are presented in section V.

## II. ONE DIMENSIONAL FUSION MODEL

### A. A diffusion model for fusion

First, we consider an one dimensional diffusion model under the influence of a linear driving force ($F = 2bR$) corresponding to a parabolic potential,

$$V_{ad} = B - b\left(R - R_b^{ad}\right)^2, \tag{1}$$

where $B$ is the barrier height at $R = R_b^{ad}$. Note that we have introduced the notation $ad$ to indicate the adiabatic nature of the potential and to make it distinguish from the sudden (frozen density approximation) potential which is generally used to describe the fusion trajectory. For example, the potenial shown in fig. 1 is commonly refered as sudden potential and is more appropriate to describe reaction dynamics when the relative motion between two colliding nuclei is fast enough as compared to other intrinsic degrees of freedom. Under this sudden or frozen density approximation, the potential depends only on the relative separation between the two colliding nuclei. However, due to neutron flow, if the colliding system forms a di-nuclear complex at $R > R_b^{ad}$, the potential is no longer a function of relative separation alone, but also it depends on the neck degree of freedom (two nuclei connected by a thin neck). The resulting fusion trajectory will be more adiabatic in nature and needs to be obtained by optimizing a set of nuclear shape parameters, a procedure what is generally adopted to obtain a conditional fission trajectory. However, we expect this adiabatic fusion trajectory to be quite different from a true fission trajectory at least in the exterior region as in case of fusion, the neck growth is not as rigorous as in the case of fission process. Although it will be interesting to estimate the fusion trajectory by parametrizing the potential in terms of a set of shape parameters that can

generate various di-nuclear configurations, in the present work, we keep the formulation simple by consideaing a parabolic form of potential as given by Eq.(1). Thus, we denote $V_b$ for sudden barrier height where as $B$ represents the height of the adiabatic potential barrier.

Defining $W(R,t)$ as the probability of finding a Brownian particle at position $R$ and time $t$, the equation describing the drift and spreading of $W(R,t)$ is given by Smoluchowski diffusion equation which is a special case of a Fokker-Plank equation [20, 21],

$$\partial_t W(R,t) = D\partial_R(\partial_R - F/\Gamma)W(R,t), \tag{2}$$

where $\partial_R$ is the partial derivative with respect to $R$, $\Gamma$ is temperature, $F = 2bR$ is the driving force and $D$ is the diffusion coefficient. The distribution $W(R,t)$ satisfies the initial condition at $R = R_0$ and $t = t_0$,

$$W(R,t_0) = \delta(R - R_0). \tag{3}$$

The above equation has a stnadard solution [20, 21] given by,

$$W(x,t) = \frac{1}{\sqrt{2\pi\xi}} exp\left[-\frac{(x- < x >)^2}{2\xi}\right], \tag{4}$$

where $x = R - R_b^{ad}$,

$$< x >= R_0\ exp\ \left[\frac{2bD}{\Gamma}(t-t_0)\right], \tag{5}$$

and

$$\xi = \frac{\Gamma}{b}\left[\ exp\ \left(\frac{4bD}{\Gamma}(t-t_0)\right) - 1\right]. \tag{6}$$

Note that both width $\xi$ and average position $< x >$ increase with time as expected, but the ratio $< x > /\sqrt{2\xi}$ approaches a constant value of $R_0\sqrt{b/\Gamma}$ as $t \rightarrow \infty$. The fusion probability can be estimated by integrating $W(x,t)$ from $x = -\infty$ to $x = 0$ (i.e. $R = -\infty$ to $R = R_b$) and taking the limit $t \rightarrow \infty$, which turns out to be,

$$T_d = \frac{1}{2}\left[1 \mp erf(Z)\right], \tag{7}$$

where $erf$ is the error function and the argument

$$Z = \sqrt{\frac{b(R_0 - R_b)^2}{\Gamma}} = \sqrt{\frac{\Delta B}{\Gamma}}. \tag{8}$$

The minus (plus) sign corresponds to the case when the injection point $R_0 > R_b$ ($R_0 < R_b$). The $\Delta B$ is the height of the barrier seen at the injection point $R_0$.

We describe the fusion of two colliding nuclei in the following way. Initially, the relative motion of two nuclei are fast enough, the role of neutron flow or the neck opening may not play a significant role and the colliding system follows a fusion trajectory which is sudden in nature. However, at the classical turning point, the system comes to the rest, developes a neck forming a di-nuclear complex and gets captured into a trajectory which is adiabatic in nature. Depending on the injection point, the system will undergo further diffusion. Fusion is achieved by diffusing up hill of the adibatic trajectory which has a barrier height $\Delta B$ at the injection point $R_0$. Since we assume $R_0$ as same as the classical turning point, it can be obtained numerically by equating $E$ with the sudden potential $V^{sud}(R)$ at $R = R_0$. However, for mathematical convenience, we parametrize this potential by using a more generic form,

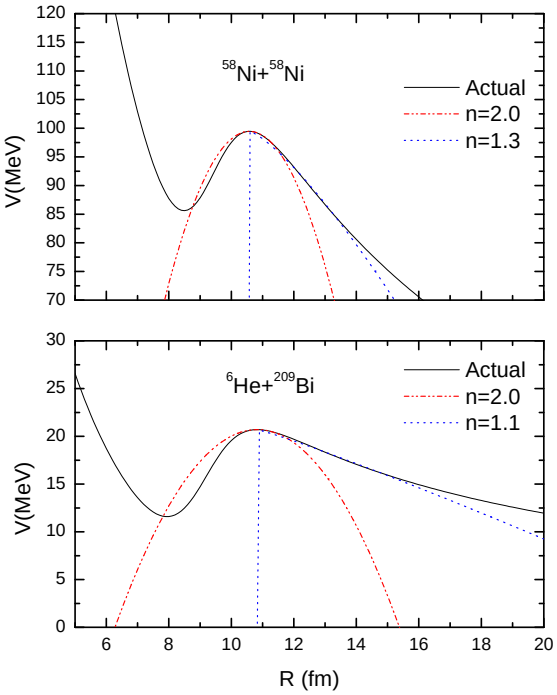


FIG. 3: The upper panel shows actual sudden potenial $V(R)$ as a function of $R$ for $^{58}Ni + ^{58}Ni$ system (solid curve). The dashed-dot curve (in red) is obtained with a fit parameter $n = 1.3$. The dotted curve (in blue) represents a parabolic potential for $n = 2.0$. The parameter $c = 4.0$ is chosen to get the fit as close as to the actual potential. The lower panel shows the similar plot for $^{6}He + ^{209}Bi$ system with $n = 1.1$ and $c = 1.0$.

$$V_{sud} = V_b - c\ (R - R_b^{sud})^n, \tag{9}$$

where $R_b^{sud}$ is the position of the sudden barrier $V_b$. The fit parameter $n$ is adjusted to reproduce the sudden potential in the outer region ($R > R_b^{sud}$). Using the above parametrization, $R_0$ can be written as,

$$R_0 = R_b^{sud} + \left(\frac{V_b - E}{c}\right)^{1/n}. \tag{10}$$

Fig. 3 shows the plots of a realistic sudden potentials (solid curves) for two typical $^{58}Ni + ^{58}Ni$ and $^{6}He + ^{209}Bi$

systems. The dashed-dot curves (in red) are obtained with the fit parameters $n = 1.3$ and $n = 1.1$ respectively. It may be pointed out here that for $n = 2$, the potential is parabolic which is most commonly used in the literature. However, we have seen a parabolic approximation grossly underestimate the potential at large distances ($R > R_b^{sud}$). It is noticed that for most of the systems in the region $R > R_b^{sud}$, the sudden potential can be approximated with the parameter $n$ which lies in the range $1 < n < 1.3$ i.e the tail of the potential more closely follows a linear decrease, rather than parabolic. It is also assumed that the injection point is same as the classical turning point $R_0$ at which the relative velocity becomes zero. This assumption is an over simplification as the capture into the adiabatic trajectory due to neck formation may take place even before the system comes to complete halt i.e. even before $R_0$ is reached. Therefore, $n$ can be kept as a fit parameter. However, it is observed that experimental data can be reproduced well when $n$ is close to unity ($n \leq 1.0$). Thus with the choice of $n = 1.0$ and using Eq.(10), the argument $Z$ in Eq.(8) can finally be written as,

$$Z = \frac{(V_b - E + \delta)}{d\sqrt{\Gamma}}, \tag{11}$$

where $d = c/\sqrt{b}$ and $\delta = c(R_b^{sud} - R_b^{ad})$. The term $\delta$ can be droped out under the assumption $R_b^{sud} = R_b^{ad}$. Even if $R_b^{sud} \neq R_b^{ad}$, $\delta$ can be taken as small energy independent positive correction which can be absorbed by redifining the sudden potential $V_b' = V_b + \delta$. However, in the present work, we will ignore this $\delta$ term i.e. we will assume that both sudden and adiabatic trajectories have the same barrier position $R_b$ although the corresponding barrier heights $V_b$ and $B$ are different. In any case (with or without $\delta$), it is interesting to note that although Eq.(7) refers to the diffusion probability over an adibatic barrier of height $B$, the argument $Z$ contains only the sudden barrier height $V_b$. This is because, in the present formalism, the adiabatic barrier height $\sqrt{\Delta B}$ as seen from the injection point $R_0$ is proportional to the height $(V_b - E)/d$. This is an important consequence of our model as the diffusion probability is still governed by the sudden barrier $V_b$, adiabatic effect enters obly through the parameter $d$. Substituting $y = -Z$ and using the property $erf(-y) = -erf(y)$, Eq.(7) can be written as a single equation,

$$T^d(E) = \frac{1}{2}\left[1 + erf(y)\right], \tag{12}$$

where $y = (E - V_b)/d$. The above equation gives only $s-$wave diffusion probablity. The $l-$dependent diffusion probability can be calculated by replacing $V_b$ with $V_b^l = V_b + l(l+1)\hbar^2/(2\mu R_b^2)$.

TABLE II: The various parameters $V_b$, $R_b$, $\hbar\omega$ and $d$ used to fit the data for five systems considered in this work. The last column shows the $\eta_0$ values used in $S(E)$ for normalization. Note that the values of $V_b$ and $R_b$ used to fit the data and the values used in table I are different due to different nuclear normalization factors. In table I, $V_b$ and $R_b$ are same as used in Ref.[4], where as, to fit the experimantal data using CCBPM and CCDIFFUSION, a different set of $V_b$ and $R_b$ are used. For all the systems except $^{64}Ni + ^{64}Ni$, we use same $V_b$ both for CCBPM and XXDIFFUSION calculations. Hoeever, for $^{64}Ni + ^{64}Ni$ system, we found a slightly lower barrier explains the data well. So we have used $V_b = 94.9$ MeV for CCDIFFUSION and $V_b = 94.5$ MeV for CCBPM.

| System | $V_b$(MeV) | $R_b$ (fm) | $\hbar\omega$(MeV) | $d$ | $\eta_0$ |
|---|---|---|---|---|---|
| $^{58}Ni + ^{58}Ni$ | 99.5 | 10.6 | 3.9 | 1.2 | 69.99 |
| $^{64}Ni + ^{64}Ni$ | 94.9(94.5) | 11.2 | 3.7 | 1.5 | 75.23 |
| $^{16}O + ^{144}Sm$ | 60.9 | 11.0 | 4.6 | 1.5 | 41.0 |
| $^{6}He + ^{209}Bi$ | 20.7 | 10.8 | 4.2 | 5.0 | 17.2 |
| $^{6}He + ^{238}U$ | 22.8 | 10.9 | 4.2 | 3.8 | 18.5 |

### B. Fusion through tunneling

We can also estimate the transmission probability through barrier penetration using the WKB approximation,

$$T_l^w(E) = \left[1 + exp(A_l)\right], \tag{13}$$

where $A_l$ is the classical action given by,

$$A_l = \frac{2\mu}{\hbar^2}\int_{R_1}^{R_2}\left(V_l(R) - E\right)dR, \tag{14}$$

and

$$V_l(R) = V_C(R) + V_N(R) + \frac{l(l+1)\hbar^2}{2\mu R^2}. \tag{15}$$

Under the parabolic approximation, Eq.(13) can also be estimated using Hill-Wheeler expression [22],

$$T_l^b(E) = \left[1 + exp\left(\frac{2\pi}{\hbar\omega}(V_b^l - E)\right)\right]^{-1}. \tag{16}$$

Finally, we can estimate the fusion cross section from the relation,

$$\sigma_f = \sum_l \sigma_l = \frac{\pi}{k^2}\sum_l (2l+1)T_l(E), \tag{17}$$

where $k$ is the relative wave number and $T_l(E)$ is the transmission probability for which either Eq.(12) or Eq.(13) can be used. Even Eq.(16) can also be used to estimate fusion cross section under parabolic approximation.

### C. Fusion cross section

In the following, we estimate fusion cross sections using one dimensional barrier penetration and diffusion

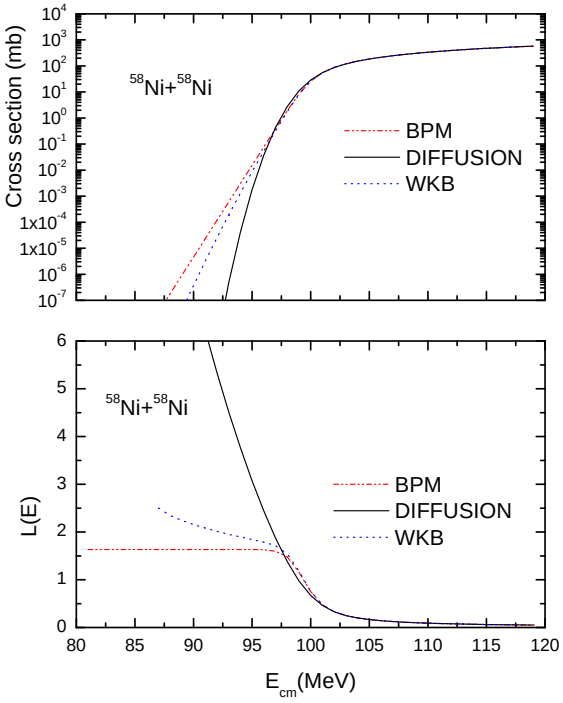


FIG. 4: (Upper panel) Fusion cross section as a function of $E_{cm}$ for $^{58}Ni+^{58}Ni$ system calculated using one dimensional barrier penetration (both WKB and BPM) and diffusion models. The barrier parameters are $V_0 = 99.5$ MeV, $R_0 = 10.6$ fm and $\hbar\omega = 3.9$ MeV for BPM calculations where as $d = 1.4$ is used in diffusion calculation in order to have similar cross section at above barrier energies. Lower panel shows corresponding $L(E)$ versus $E_{cm}$ for the same system.

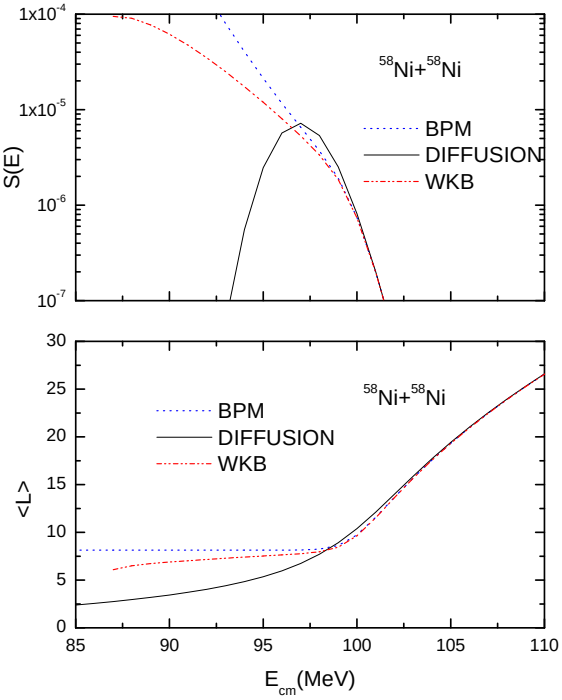


FIG. 5: The $S$ factor versus $E_{cm}$ (upper panel) and $< L >$ versus $E_{cm}$ (lower panel) for $^{58}Ni+^{58}Ni$ system using BPM,WKB and diffusion models. The potential and diffusion parameters are same as that of figure 4.

model. Under the barrier penetration model, we will use both WKB (Eq.(13)) as well as parabolic approximation (Eq.(16)). The later approximation in the text is refered as BPM model which has three parameters, the barrier height $V_b$, the barrier width $\hbar\omega$ and barrier position $R_b$. The diffusion model has also three parameters, $V_b$, $R_b$ and $d$. While $V_b$ and $R_b$ are taken same as that of BPM parameters, the $d$ parameter is adjusted to reproduce the experimental measurements. The temperature $\Gamma$ is obtained from the relation $E^* = a\Gamma^2$ where $E^*$ is the excitation energy and $a$ is the level density parameter which is taken as $(A_1 + A_2)/10$. Fig.4 shows the fusion cross section for a typical $^{58}Ni+^{58}Ni$ system using WKB, BPM and diffusion models. The potential parameters are given in table II. The dotted curve (in blue) is obtained using the BPM (parabolic barrier penetration model) where as the dashed-dot (in red) curve is an exact WKB calculation. The solid curve is obtained using diffusion model with the same barrier parameters as that of BPM but $d$ is adjusted so as to have same fusion cross section at above barrier energies. The lower pannel shows the corresponding logarithimic derivatives which is defined as

$$L(E) = \frac{d[ln(E\sigma)]}{dE}. \tag{18}$$

It is interesting to note that $L(E)$ in BPM model saturates to a constant value, where as WKB calculation shows a slow rise with decreasing energy. Contrary to both WKB and BPM calculations, the diffusion model result shows a steep rise in $L(E)$ as energy decreases. This is also evident from the upper panel as fusion cross section in diffusion model falls off more steeply at deep-subbarrier energies, although both BPM and diffusion models give nearly same cross section at near and above barrier energies. Another pragmatic way to represent the fusion process at sub-barrier energy is the $S$ factor which is defined as

$$S(E) = E\sigma e^{2\pi(\eta-\eta_0)}, \tag{19}$$

where $\eta = Z_1 Z_2 e^2/(\hbar v)$ is the Sommerfeld parameter and $v$ is the beam velocity. Fig. 5 shows the plot of $S$ factors obtained using BPM, WKB and Diffusion models. For sack of completeness, the lower panel also shows another measurable quantity, the average angular momentum $< l >$ as a function of energy $E_{cm}$. The average $< l >$ is defined as,

$$< l >= \frac{\sum l\ \sigma_l}{\sigma_f}, \tag{20}$$

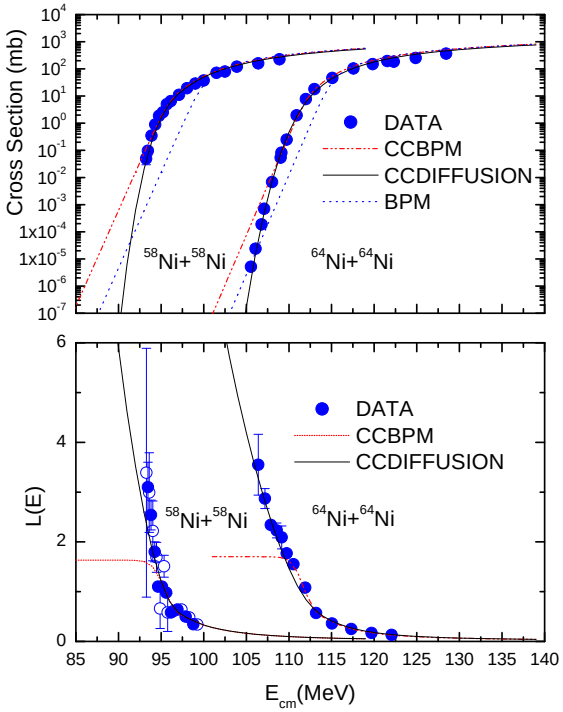


FIG. 6: Fusion cross section (upper panel) and $L(E)$ versus $E_{cm}$ (lower panel) for $^{58}Ni+^{58}Ni$ and $^{64}Ni+^{64}Ni$ systems. The potential parameters are listed in table II. The lower panel shows the corresponding $L(E)$ as a function of $E_{cm}$ for the same systems. The data points are taken from [4, 5]. For $^{64}Ni+^{64}Ni$, the X-axis is shifted by +20 MeV for clarity.

It is interesting to note that the $S$ factor in diffusion model shows a well defined maxima at deep sub-barrier energy (see Fig. 5), a feature which is supported by experimental measurements. On the other hand, $S$ factor obtained using barrier penetration models (either WKB or BPM) keeps on increasing with decreasing energy. Similarly, the average $< l >$ value shows saturation at deep sub-barrier energy where as $< l >$ obtained using diffusion model decreases with energy without having any saturation point. As the above models are one dimensional in nature, we do not compare the results with the experimental measurements. We only show it to demonstrate that the diffusion model has certain basic features at deep sub-barrier energies which are consistent with experimental observations and can not be reproduced by any type of barrier penetration models with the same type of potential as used in the diffusion model.

## III. COUPLED CHANNEL CALCLATION

So far, we have considered transmission either through diffusion or through barrier penetration only from a single barrier. It is now well known that channel coupling plays an important role in heavy ion fusion enhancement particularly at sub-barrier energies. Although, there are several ways to carry out coupled channel calculations, here we adopt a very simple approach as originally suggested in [23] followed by the computer code CCFUS [24]. In this approach, instead of a single barrier $V_b$, the fusing system encounters a distribution of eigen barriers (or eigen channel $\alpha$) with probability $\omega_\alpha$. The total fusion cross section is written as the weighted sum of the fusion cross sections over all the eigen channels $\alpha$ and is given by,

$$\sigma_f = \sum_\alpha \omega_\alpha \sigma_f(V_b^\alpha, E), \tag{21}$$

where $\omega_\alpha$ is the weight factor for channel $\alpha$ and $\sigma_f(V_b^\alpha, E)$ is the corresponding fusion cross section in channel $\alpha$ which has a barrier height $V_b^\alpha$, In our formalism, since the system encounters both sudden and adiabatic trajectories, we would like to argue here that the inelastic coupling (vibrational or rotational) will affect only the sudden trajectory while the adiabatic trajectory by and large will remain unaffected. As an example, in case of static deformation of the nuclei, the fusion barrier depends on the projectle-target orientation and the total fusion cross section is written as the weighted sum over all the angles. Microscopically, it is equivalent to the rotational couplings under the approximation of zero intrinsic excitation energies. However, if the projectile and target form a di-nuclear complex due to neck formation, the resulting adiabatic trajectory will be insensitive to the initial deformation effect as it is obtained by optimizing a set of nuclear shape parameters. Therefore, when the sudden tajectory is replaced by a distribution of eigen trajectories due to channel couplings, it has no direct effect on the adiabatic trajectory. However, the injection point which is the same as the classical turning point $R_0$ will now be channel dependent and needs to be replaced by a distribution of injection points depending on the channel $\alpha$. Since $R_0$ depends on $R_b + (V_b - E)$, $\sqrt{\Delta B^\alpha}$ should also be replaced by $(V_b^\alpha - E)$ for each channel $\alpha$ with the same weight factor $\omega_\alpha$. The net effect is that the diffusion probabilty will also be different depending on the eigen channel $\alpha$.

In the computer code CCFUS, the transmission propobaility from a single barrier is used using the Hill-Wheeler barrier penetration factor $T^b$ given by Eq.(16), We can use the same CCFUS code by replacing $T^b$ by the diffusion probability $T^d$ as given by Eq.(12). In fact, we will use both the factors $T^b$ (to be refered as CCBPM) and $T^d$ (to be refered as CCDIFFUSION). We consider $2^+$ , $3^-$ and $4^+$ inelastic states of $^{58}Ni$ and $^{64}Ni$ with the same coupling parameters as given in [23]. For the CCBPM calculations, we have as usual three parameters $V_b$, $R_b$ and $\hbar\omega$ and the values used in this work are listed in table II. In CCDIFFUSION, we use the same value of $V_b$ and $R_b$ as CCBPM, but adjust the variable $d$ to reproduce the experimental data. For $^{58}Ni+^{58}Ni$ system, the $V_b$, $\hbar\omega$ , $R_b$ and $d$ values are 99.5 MeV, 3.9

MeV, 10.6 fm and 1.2 respectively. The same set of parameters are used both in CCBPM and CCDIFFUSION calculations. However, for $^{64}Ni + ^{64}Ni$ system, we use $V_b = 94.9$ MeV, $\hbar = 3.7$ MeV, $R_b = 11.2$ fm and $d = 1.5$ for CCDIFFUSION calculations. For CCBPM, we have noticed a slight lower value of $V_b$ gives better result. Accordingly, we use $V_b = 94.5$ MeV for CCBPM where as all other parameters are kept same as that of CCDIFFUSION. Fig.e (6) (upper panel) shows fusion cross sections for the above two systems using coupled channel calculation with both CCBPM (dashed dot curve in red) and CCDIFFUSION(solid curve). The one dimensional BPM model without any coupling effect has also been shown for comparison (dotted curve in blue). As expected, the BPM model underestimates the fusion cross section at sub-barrier energies. The CCBPM accounts for the fusion enhancement at sub-barrier eneries, it over predicts the fusion cross section at deep sub-barrier energies. The important observation is that the $L(E)$ obtained from the CCBPM model (see the lower panel) tends to saturate to a constant value at deep sub-barrier energies like the BPM model as shown in Fig. 4. However, the prediction of CCDIFFUSION explains the data quite well both at sub-narrier as well as at deep sub-barrier energeis. It also expalins the general trend of $L(E)$ which keeps on increasing with decreasing energy.

Fig. 7 shows the $S(E)$ factors (upper panel) for the above two systems. The normalisation factors $\eta_0$ are 69.99 for $^{58}Ni + ^{58}Ni$ system and 75.23 for $^{64}Ni + ^{64}Ni$ system. As shown in the figure, the predictions of CCDIFFUSION are in excellent agreement with the observed $S$ factors where as CCBPM keeps on increasing without showing the maxima. The lower panel shows the $< l >$ as a function of energy. In addition to $^{58}Ni + ^{58}Ni$ system, we have also estimated $< l >$ distribution for $^{16}O + ^{144}Sm$ system. In the coupling scheme, we include only a $3^-$ inelastic state of $^{16}O$ with $\beta = 1.81$ and excitation energy $E^* == 0.25$ MeV. As will be shown in next section, this coupling is sufficient to reproduce the fusion cross section and measured barrier distribution. It is interesting to note that while both BPM and CCBPM predict a saturation value, CCDIFFUSION model does not show any saturation point. The $< l >$ decreases with decreasing energy. This aspect can be verified experimentally if possible by extending the measurements to lower energies.

Like $L(E)$ and $S(E)$, another pragmatic way to represent fusion data is through it's second derivative given by the relation,

$$D(E) = \frac{1}{\pi R_b^2} \frac{d^2(\sigma_f E)}{dE^2}, \tag{22}$$

which is interpreted as the experimental barrier distribution smeared by a tunneling or transmission factor. Assuming $T_l(E) = T_0(\epsilon)$ where $\epsilon = E - l(l+1)\hbar^2/(\mu R_b^2)$, it can be shown that

$$T_0(E) = \frac{1}{\pi R_b^2} \frac{d(\sigma E)}{dE}. \tag{23}$$

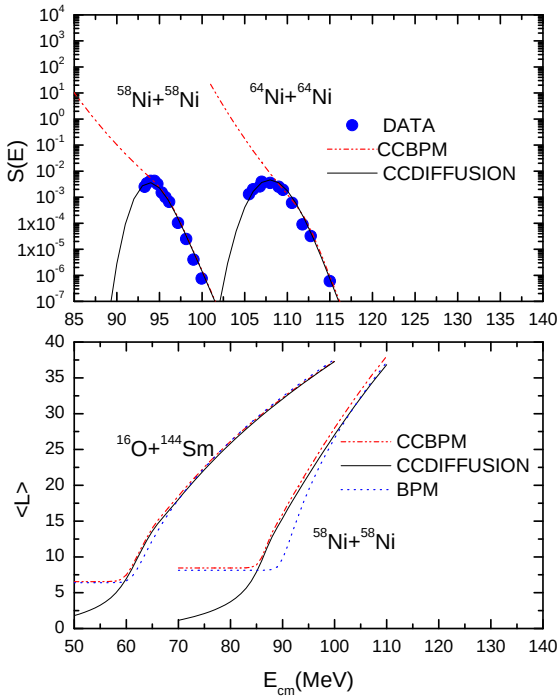


FIG. 7: The $S$ factor as a function of $E_{cm}$ (upper panel) for the same systems as shown in figure 6. For $^{64}Ni + ^{64}Ni$, the X-axis is shifted by +20 MeV for clarity. The lower panel shows $< L >$ as a function of $E_{cm}$ for $^{16}O + ^{144}Sm$ and $^{58}Ni + ^{58}Ni$ systems. The potential parameters are listed in table I. For $^{58}Ni + ^{58}Ni$, the X-axis is shifted by $-10$ MeV for clarity.

Therefore, in case of a single barrier, the fusion cross section can be obtained by integrating the above equation form 0 to $E$ and using $T_0(E)$ either from Eq.(16) or Eq.(12). In the first case,

$$\sigma_f(E, V_b) = \frac{\pi R_b^2}{E} log\left[1 + exp\left\{\frac{2\pi}{\hbar\omega}(E - V_b)\right\}\right]. \tag{24}$$

where as in the second case,

$$\sigma_f(E, V_b) = \pi R_b^2 \frac{\gamma}{E\sqrt{2\pi}}\left[X\sqrt{\pi}\,(1 + erf\ X) + exp\,(-X)\right] \tag{25}$$

where

$$X = \frac{E - V_b}{\sqrt{2}\gamma} \tag{26}$$

and $d\sqrt{\Gamma} = \sqrt{2}\gamma$ is assumed as constant. Note that while both Eq.(24) and Eq.(25) are the expressions for one dimensional fusion cross section models, Eq.(24) represents the celebrated Wong's formulae under parabolic approximation (BPM ) [25] where as Eq.(25) is identical to the expression used by Wilczynska and Wilczynski (See Eq. 6 of Ref.[26]) to fit fusion cross section for several heavy ion systems.

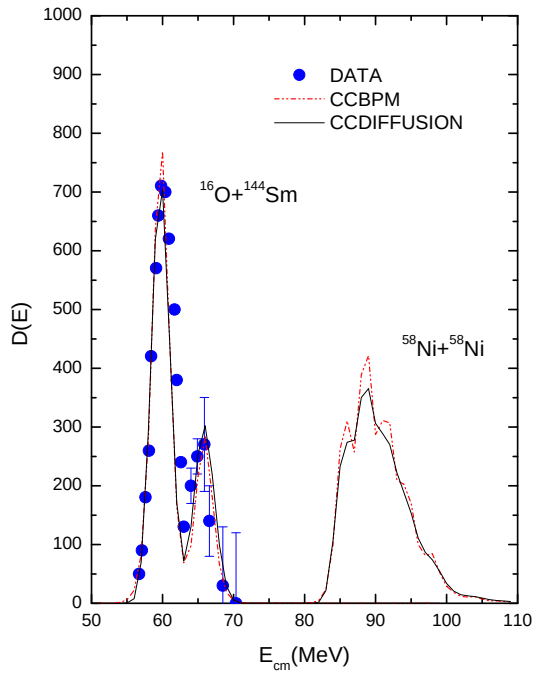


FIG. 8: The $D(E)$ versus $E_{cm}$ for $^{16}O+^{144}Sm$ and $^{58}Ni+^{58}Ni$ systems. The data points are taken from Ref. [27]. The X-axis is shifted by $-10$ MeV for $^{58}Ni+^{58}Ni$ system for clarity.

The fusion cross section in Eq. (21) is written as the sum over the discrete barriers. Replacing this sum by an integral i.e. replacing the weight $\omega_\alpha$ by a distribution of barriers with probablity $D(V)$ and using fusion cross section from Eq.(24), it can be shown that

$$\frac{1}{\pi R_b^2}\frac{d^2(\sigma_f E)}{dE^2} = \int_0^E D(V)G(f)dV, \tag{27}$$

where

$$G(f) = \frac{dT_0}{dE} = \left(\frac{2\pi}{\hbar\omega}\right)\frac{exp(f)}{[1+exp(f)]^{-2}}, \tag{28}$$

and

$$f = \left(\frac{2\pi}{\hbar\omega}\right)(E-V). \tag{29}$$

If $G(f)$, which is a sharply peaking function at $E=V$, can be replaced by a delta function $\delta(E-V)$, Eq.(27) represents a true barrier distrbution as given by Eq.(22). However, the above interpretation breaks down if we replace $T_0(E)$ by Eq.(12). In case of diffusion,

$$G(f) = \frac{dT_0}{dE} = \frac{1}{\gamma\sqrt{2\pi}}exp\left[-\frac{(E-V)^2}{2\gamma^2}\right], \tag{30}$$

which is a Gaussian instead of a delta function and it will not be appropriate to interprete Eq.(27) as barrier distribution. Since all experimental measurements derived using Eq.(22) are associated with true barrier distribution, it should be interpreted with some amount of caution. On the other hand, whatever be the interpretation, like $L(E)$ and $S(E)$, $D(E)$ is another meaningful representation of experimental data which is very sensitive to the coupling parameters (hence to the nuclear structure effects) at and above the barrier region. Fig. 8 shows $D(E)$ for $^{16}O+^{144}Sm$ and $^{58}Ni+^{58}Ni$ systems with the same coupling parameters as discussed before. The experimental barrier distributions are shown only for $^{16}O+^{144}Sm$ system. As can be seen, the predictions of both CCBPM and CCDIFFUSION are nearly identical and also both show the nuclear structure effects at and above barrier energies. Although $\sigma_f$ at deep sub-barrier energy is different for both CCBPM and CCDIFFUSION , the $D(E)$ is not sensitive to this varitioan. It may be mentioned here that unlike $D(E)$, both $L(E)$ and $S(E)$ strongly depend on the variation of fusion cross sections at deep sub-barrier energeis. Therefore, any model, to remain valid from above barrier to deep sub-barrier energies, it should account for the above three factors simultaneously.

Finally, we would like to mention here that although Eq.(25) is identical to the expression used in Ref.[26], the interpretations under which it has been derived are quite different. For example, the authors of Ref.[26] start with a classical expression for fusion,

$$\sigma_f = \pi R_b^2(1-\frac{V_b}{E}), \tag{31}$$

which gives,

$$\frac{1}{\pi R_b^2}\frac{d^2(E\sigma)}{dE^2} = \delta(V_b - E). \tag{32}$$

Eq. (25 can be obtained by replacing this delta function by a Gaussian distribution of barrier,

$$\rho(V) = \frac{1}{\gamma\sqrt{2\pi}}exp\left[-\frac{(E-V_b)^2}{2\gamma^2}\right], \tag{33}$$

and integrating from 0 to $E$. Using Eq.(25) and with $V_b$, $R_b$ and $\gamma$ as parameters, the authors of Ref.[26] have fitted fusion cross sections for several systems over a wide range of energies. Although, they are able to fit the data for several systems, the parameters turns out unphysical. For example, the $R_b$ value for $^{58}Ni+^{58}Ni$ is found out to be 6.0 fm where as the normal value is about 10.5 fm. Since the fusion cross section approaches its geometrical limit at higher energies ($\sigma_f = \pi R_b^2$), the reduced radius parameter would result in a cross section which will be about 30% less. This unphysical behaviour is probably due to forcing an one diemnsional model to explain the fusion data over a wide range without using any channel coupling effects.

## IV. FUSION OF RADIO ACTIVE IONS

In recent years, much efforts have been devoted to study the fusion reaction of light halo nuclei with stable

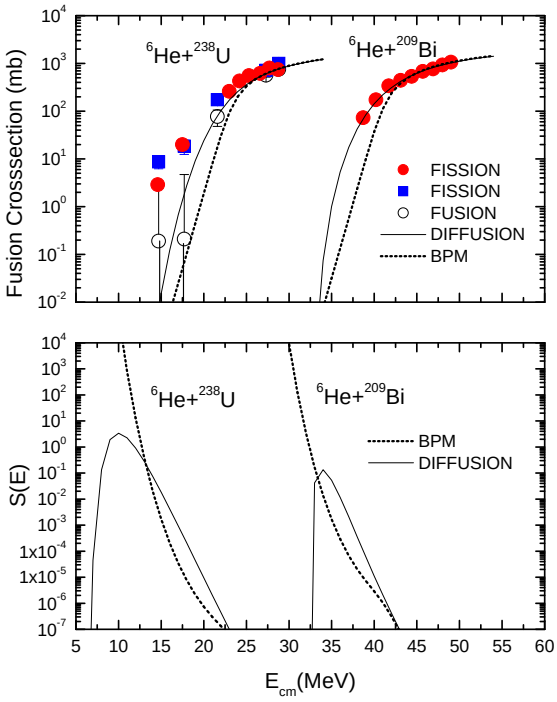


FIG. 9: The fusion cross section versus $E_{cm}$ for $^6He+^{238}U$ and $^6He+^{209}Bi$ systems and their corresponding $S$ factors. The potential parameters are listed in table II. The experimental data points for $^6He+^{209}Bi$ system are taken from Ref.[11]. For $^6He+^{238}U$, the fission and fusion data points (squares and open circles) are taken from Ref.[14] and the solid circles (normalized by a factor of 0.54 as suggested in Ref.[14]) are taken from Ref.[13]. The X-axis for $^6He+^{209}Bi$ system is shifted by $-10$ MeV for clarity.

heavy targets at energy around the Coulomb barrier. In light exotic nuclei such as $^6He$, $^{11}Li$ and $^{11}Be$, the neutron matter extends to a larger distance than the usual nuclear interaction scale. The fusion cross section for such system is expected to be enhanced with respect to the fusion with stable projectile due to the reduction in Coulomb barrier. On the other hand, the weak binding of the halo neutrons lead to a higher break up probability of the projectile, which in turn, reduces the fusion cross section. Therefore, understanding the effect of neutron halo on fusion has been highly contoversial. In one of the earlier measurements in $^6He+^{209}Bi$ reaction, a significance enhancement in fusion cross section with respect to $^4He+^{209}Bi$ system was observed, especially at sub-barrier region [11]. In the subsequent study [12], an isolated $^4He$ group was observed with cross section far exceeding the fusion yield both above and below the barrier. This reaction mechanism was interpreted as the direct break up and transfer of neutrons to the unbound states in $^{211}Bi$, a mechanism having close resembalnce to neutron flow [17]. The effect of the halo on the fusion-fission probabilty was also measured for $^6He+^{238}U$ system [13]. The data lead to the conclusion that there is no hindrance to fusion at the barrier due to break up reaction and below barrier, there is a large enhancement of the fusion probability for the $^6He$ nucleus with respect to stable $^4He$ (see filled circles and squares in Fig. 9). However, this measureemnt was confronted later on as no substantial fusion enhancement was observed [14], rather, the large fusion yield was found due to two neutron tranfer induced fission of $^{240}U$ (The open circles in Fig. 9 which are obtained after correcting for transfer induced fission). It was also concluded that a simple BPM model may be adequate to explain the data. Recently, the yield of $^{210}Po$ isotope has been measured through the $2n$ evaporation channel of the fusion reaction $^6He$ with the $^{208}Pb$ target [15]. The yield demonstrates an extremely large enhancement of sub-barrier fusion cross section. Such a controversial situation in the experimental data on sub-barrier reaction as it has been in the theoretical interpretations.

Although we are still far from good understanding of the subject and much more experimental and theoretical studies are needed, in the following we examine the possibility of explaining the fusion reaction involving halo nuclei based on the same diffusion model which has been used for heavy ion systems. Due to the extended neutron distribution, it is more probable that the system forms a di-nuclear complex at a large distance due to sequential neutron flow promoting neck formation. Thus, instead of tunneling, the di-nuclear configuration will diffuse over an adiabatic barrier in order to achieve fusion. Since the projectile is light, there should not be any coupling effect except the neck formation. The fusion process should follow an one dimensional diffusion model as given by Eq.(17) with diffusion probability as given by Eq.(12). Fig.9 shows $\sigma_f$ as a function of $E_{cm}$ for $^6He+^{238}U$ and $^6He+^{209}Bi$ systems. The dotted curves show the predictions based on the BPM model which has three parameters, $V_b, R_b, \hbar\omega$. The diffusion model uses the same $V_b$ and $R_b$ parameters, but the $d$ is adjusted to get a reasonably good fit to the experimental data points. The lower panel shows the expected $S$ factors.

## V. CONCLUSION

In conclusion, we have proposed a new model based on the diffusion over an adibatic fusion trajectory to explain fusion cross section $\sigma_f$ and associated derived quantities like $L(E)$, $S(E)$ and $D(E)$ for several systems both at above and below barrier energies. For the fusion of light projectile with heavy target for which neck fromation or neutron flow is not very meaningful (like fusion of $^4He$ on stable neuclei), the system will fuse through one dimensional tunneling of the sudden barrier and the fusion cross section can be described by Wong type calculation (a simple BPM model). However, if the projectile is a halo nuclei, but still lighter enough so that coupling effects can be neglected (as coupling potential depends on

$Z_1 Z_2$), the fusion need to proceed through diffusion. Similarly, for heavy projectile target combinations, coupled channel calculations are required to be carried out with diffusion as the mechanism of transmission over the adiabatic Coulomb barrier.


[1] A. B. Balantekin, and N. Takigawa, Rev. Mod. Phys. **70**, 77 (1998),

[2] M. Dasgupta et al, Annu. Rev. Nucl. Part. Sci. **48**, 401 (1998).

[3] N. Rowley, G. R. Satchler, and P. H. Stelson, Phy. Lett. **B254**, 25 (1991).

[4] C. L. Jiang et al, Phys. Rev. Lett, **89**, 052701 (2002), C. J. Lin, ibid. **91**, 229201 (2003), C. L. Jiang et al ibid. **91**, 229202 (2003) .

[5] C. L. Jiang et al, Phys. Rev. Lett, **93**, 012701 (2004),

[6] K. Hagino, N. Rowley, and M. Dasgupta, Phys. Rev. C67, 054603 (2003).

[7] C. L. Jiang, H. Esbensen, B. B. back, R. V. Janssens, and K. E. Rehm, Phys. Rev. **C69**, 014604 (2004).a

[8] S. V. S. Sastry, S. Kailas, A. K. Mohanty, and A. Saxena, Pramana, J. Phys. **64**, 47 (2005).

[9] S. Misicu and H. Esbensen, Phys. Rev. Lett. **96**,112701 (2006).

[10] S. Misicu and H. Esbensen, Phys. Rev. **C75**,034606 (2007).

[11] J. J. Kolata et al, Phys. ev. Lett. **81**, 4580 (1998).

[12] E. F. Aguilera et al, Phys. ev. Lett. **84**, 5058 (2000).

[13] M. Trotta et al, Phys. ev. Lett. **84**, 2342 (2000).

[14] R. Raabe et al, Nature **431**, 823 (2004).

[15] Yu. E. Penionzhkevich, V. I. Zagrebaev, S. M. Lukyanov, and R. Kalpakchieva, Phys. ev. Lett. **84**, 2342 (2000).

[16] Yu. E. Penionzhkevich et al, Eur. Phys. J **A31**, 185 (2007).

[17] P. H. Stelson, Phy. Lett. **B205**, 190 (1988), P. H. Stelson, H. J. Kim, M. Beckerman, D. Shapira, and R. L. Robinson, Phys. Rev. **C41**, 1584 (1990).

[18] V. S. Ramamurthy, A. K. Mohanty, S. K. Kataria, and G. Rangarajan, Phy. Rev. **C41**, 2702, 1990.

[19] N. Rowley, I. J. Thompson and M. A. Nagarajan, Phys. Lett. **B282**, 276 (1992).

[20] H. Riske, *The Fokker-Plank Equation (Springer-Verlag, Berlin* 1989.

[21] W. J. Swiatecki, K. Siwek-Wilczynska, and J. Wilczynski, Acta Physica **B34**, 2049 (2003), ibid. Phys. Rev. **C71**, 014602 (2005).

[22] D. L. Hill and J. A. Wheeler, Phys. Rev. **89**, 1102 (1953).

[23] R. A. Broglia, C. H. Dasso, S. Landowne and G. Pollarolo, Phys. Lett, **133B**, 34 (1983).

[24] C. H. Dasso, S. Landowne, Comp. Phys. Commu. **46**, 187 (1987).

[25] C. Y. Wong, Phys. Rev. Lett. **31**, 766 (1973).

[26] K. Siwek-Wilczynska, and J. Wilczynski, Phys. Rev. **C69**, 024611 (2004).

[27] J. R. Leigh et al, Phys. Rev. **C52**, 3151 (1995).